

Interferometric imaging of amplitude and phase of spatial biphoton states

Received: 13 February 2023

Accepted: 11 July 2023

Published online: 14 August 2023

 Check for updatesDanilo Zia¹ , Nazanin Dehghan^{2,4}, Alessio D’Errico^{2,4}  , Fabio Sciarrino¹ & Ebrahim Karimi^{2,3} 


High-dimensional biphoton states are promising resources for quantum applications, ranging from high-dimensional quantum communications to quantum imaging. A pivotal task is fully characterizing these states, which is generally time-consuming and not scalable when projective measurement approaches are adopted; however, new advances in coincidence imaging technologies allow for overcoming these limitations by parallelizing multiple measurements. Here we introduce biphoton digital holography, in analogy to off-axis digital holography, where coincidence imaging of the superposition of an unknown state with a reference state is used to perform quantum state tomography. We apply this approach to single photons emitted by spontaneous parametric down-conversion in a nonlinear crystal when the pump photons possess various quantum states. The proposed reconstruction technique allows for a more efficient (three orders of magnitude faster) and reliable (an average fidelity of 87%) characterization of states in arbitrary spatial modes bases, compared with previously performed experiments. Multiphoton digital holography may pave the route toward efficient and accurate computational ghost imaging and high-dimensional quantum information processing.

Photonic qudits are emerging as an essential resource for environment-resilient quantum key distribution, quantum simulation and quantum imaging and metrology¹. The availability of unbounded photonic degrees of freedom, such as time-bins, temporal modes, orbital angular momentum (OAM) and radial number¹, allows for encoding large amounts of information in fewer photons than would be required by qubit-based protocols (for example, when using only polarization). At the same time, the large dimensionality of these states, such as those emerging from the generation of photon pairs, poses an intriguing challenge for what concerns their measurement. The number of projective measurements necessary for a full-state tomography scales quadratically with the dimensionality of the Hilbert space under consideration². This issue can be tackled with adaptive tomographic approaches^{3–5} or compressive techniques^{6,7}, which

are, however, constrained by a priori hypotheses on the quantum state under study. Moreover, quantum state tomography via projective measurement becomes challenging when the dimension of the quantum state is not a power of a prime number⁸. Here we try to tackle the tomographic challenge, in the specific contest of spatially correlated biphoton states, looking for an interferometric approach inspired by digital holography^{9–11}, familiar in classical optics. We show that the coincidence imaging of the superposition of two biphoton states, one unknown and one used as a reference state, allows retrieving the spatial distribution of phase and amplitude of the unknown biphoton wavefunction. Coincidence imaging can be achieved with modern electron-multiplying charged coupled device cameras^{12,13}, single photon avalanche diode arrays^{14–16} or time-stamping cameras^{17,18}. These technologies are commonly exploited in quantum imaging, such as

¹Dipartimento di Fisica, Sapienza Università di Roma, Roma, Italy. ²Nexus for Quantum Technologies, University of Ottawa, Ottawa, Ontario, Canada.

³National Research Council of Canada, Ottawa, Ontario, Canada. ⁴These authors contributed equally: Nazanin Dehghan, Alessio D’Errico.

 e-mail: aderrico@uottawa.ca

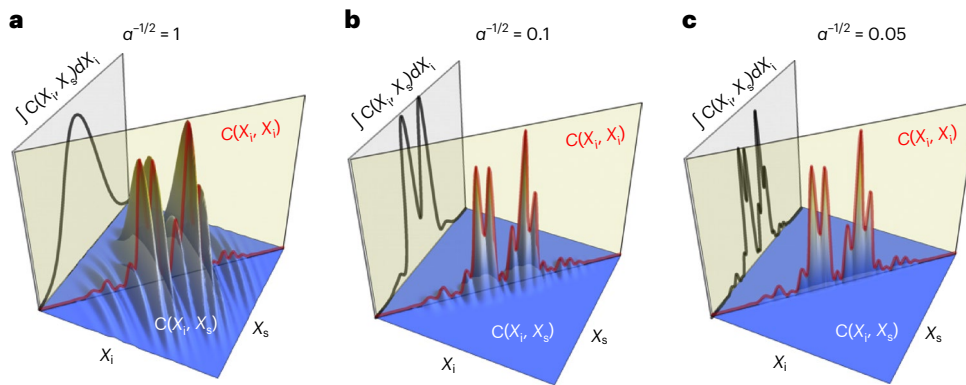


Fig. 1 | Biphoton state holographic reconstruction. Pictorial representations of equation (2) (in the simplified scenario of a two-dimensional space (X_i, X_s)) for different scenarios in which the biphoton wavefunctions have variable spatial correlations. To mimic typical SPDC states, we modelled the reference biphoton as a product $\exp(-\alpha(X_i - X_s)^2) \exp(-(X_i + X_s)^2/\sigma^2 + ik(X_i + X_s))$ and the unknown wavefunction as $\exp(-\alpha(X_i - X_s)^2) \exp(-(X_i + X_s)^2/\sigma^2) h_2((X_i + X_s)/\sigma_2)$, where $h_n(x)$ are Hermite polynomials. The parameter α quantifies the narrowness of the diagonal correlations. Alongside the three-

dimensional plot of $\mathcal{C}(X_i, X_s)$, we show the marginal correlation $\int \mathcal{C}(X_i, X_s) dX_i$ (which corresponds to the coincidence image obtained when no spatial post-selection is performed) and the section $\mathcal{C}(X_i, X_i)$, which can be obtained post-selecting on diagonal correlations. **a–c**, We chose $\sigma = 1, \sigma_2 = 0.6, k = 2\pi/(0.2\sigma)$, and $\alpha = 1$ (**a**), $\alpha = 100$ (**b**) and $\alpha = 400$ (**c**). The correlation width $1/\sqrt{\alpha}$ is reported in each pane. We see that, in the strong correlation limit (**c**), interference is also retrieved in the marginal distribution.

ghost imaging experiments¹⁹ or quantum super-resolution^{20,21}, as well as for fundamental applications, including characterizing two-photon correlations^{13,22}, imaging of high-dimensional Hong–Ou–Mandel interference^{23–25}, and visualization of the violation of Bell inequalities²⁶. Holography techniques have been recently proposed in the context of quantum imaging^{27–29}; demonstrating the phase-shifting digital holography in a coincidence imaging regime using polarization entanglement²⁷, and exploiting induced coherence, that is, the reconstruction of phase objects through digital holography of undetected photons²⁸.

In this work, we focus on the specific problem of reconstructing the quantum state (in the transverse coordinate basis) of two photons emerging from degenerate spontaneous parametric down-conversion (SPDC). These states are characterized by strong correlations in the transverse position (considered on the plane where the two-photon generation happens), which can be observed in other kinds of photon sources such as cold atoms³⁰. In these sources, the two-photon wavefunction strongly depends on the shape of the pump laser used to induce the down-conversion process³¹. The most commonly used approach in the literature to reconstruct the biphoton state emitted by a nonlinear crystal is based on projective techniques^{32–34}. This method has drawbacks concerning measurement times (as it needs successive measurements on non-orthogonal bases) and the signal loss due to diffraction. We proposed an imaging-based procedure capable of overcoming both of the issues mentioned above, while giving the full-state reconstruction of the unknown state. The core idea lies in assuming the SPDC state induced by a plane wave as known, and in superimposing this state with the unknown biphoton state. Unless the superposition is achieved directly on the crystal plane, a full analysis of the four-dimensional distribution of coincidences is necessary to retrieve the interference between the two wavefunctions. This information can be visualized by observing coincidence images, defined as marginals of the coincidence distribution obtained integrating over the coordinates of one of the two photons. In fact, obtaining coincidence images after post-selecting specific spatial correlations allows retrieval of the phase information, likewise in cases in which the state does not exhibit sharp spatial correlations. We demonstrate this technique for pump beams in different spatial modes, including Laguerre–Gaussian (LG) and Hermite–Gaussian (HG) modes. We investigate several physical effects from the

reconstructed states, such as OAM conservation, the generation of high-dimensional Bell states, parity conservation and radial correlations. Remarkably, we show how, from a simple measurement, one can retrieve information about two-photon states in arbitrary spatial mode bases without the efficiency and alignment issues that affect previously implemented projective characterization techniques. Depending on the source brightness and the required number of detection events, the measurement time can be of the order of tens of seconds, whereas the previously implemented projective techniques required several hours and were limited to the exploration of a small subspace of spatial modes. As a latter example, we give a proof of principle demonstration of the use of this technique for quantum imaging applications.

Theoretical background

We start by considering a general scenario in which the superposition between two biphoton states is created. We label each state as $|\psi_r\rangle$ and $|\psi_u\rangle$, where the subscripts r and u stand for reference and unknown, respectively. The state $|\psi_r\rangle$ is considered as known (for example, it can emerge from a source that was previously characterized), whereas the goal is finding $|\psi_u\rangle$ from measurements performed on the superposition state $|\Psi_{\text{TOT}}\rangle = |\psi_r\rangle + |\psi_u\rangle$. To simplify the analysis, we consider the case in which the photons are frequency-degenerate and with the same polarization. The biphoton states can be thus decomposed in transverse spatial degrees of freedom (or, equivalently, in the transverse momentum) as

$$|\psi_\eta\rangle = \iint d^2X_i d^2X_s \psi_\eta(\mathbf{X}_i, \mathbf{X}_s) |\mathbf{X}_i\rangle \otimes |\mathbf{X}_s\rangle, \quad (1)$$

where $\eta = r, u$; ψ_η is a complex function of the transverse coordinates of idler and signal photons $(\mathbf{X}_i, \mathbf{X}_s)$ at a given plane. The superposition state is

$$|\Psi_{\text{TOT}}\rangle = \iint d^2X_i d^2X_s [\psi_r(\mathbf{X}_i, \mathbf{X}_s) + \psi_u(\mathbf{X}_i, \mathbf{X}_s)] |\mathbf{X}_i\rangle \otimes |\mathbf{X}_s\rangle.$$

If ψ_r is known, one can retrieve information about the phase of ψ_u by coincidence measurements in the transverse position basis.

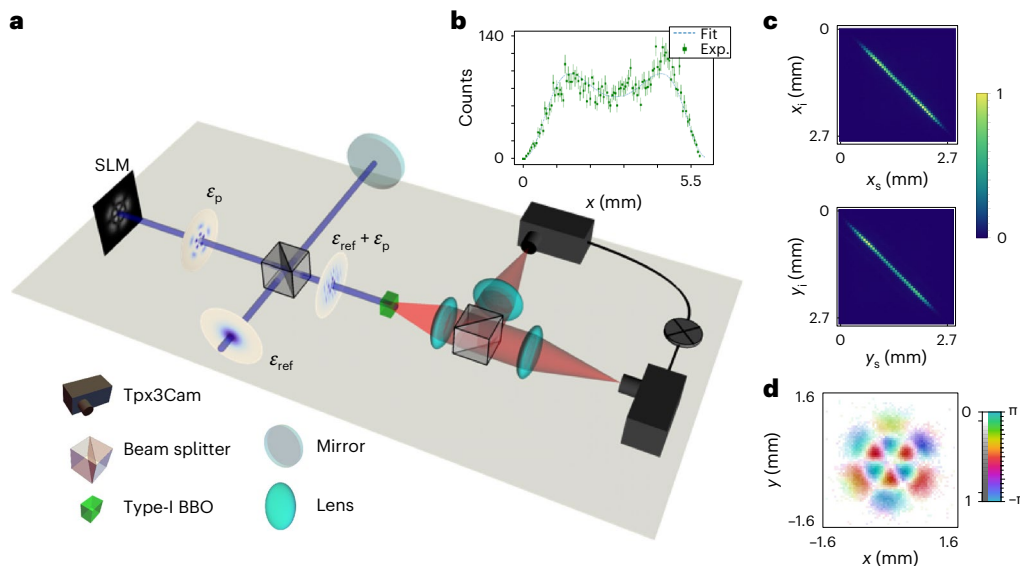


Fig. 2 | Experimental set-up and state reconstruction. **a**, Sketch of the experimental set-up: a 405 nm laser in a Gaussian mode (\mathcal{E}_{ref}) enters a Michelson interferometer, where an ultraviolet spatial light modulator (UV-SLM) in one arm is used to shape and generate the unknown pump field (\mathcal{E}_p). The interferometer's output is the superposition of the reference and unknown pump field, which is then shined on a 0.5-mm-thick type-I BBO crystal. Photon pairs are consequently generated and, after being separated through the beam splitter, sent on single photon sensor arrays. The experiment was conducted with one camera and the figure is just for illustration, a more detailed description and figure of the set-up can be found in Supplementary Information. **b**, By placing the camera in the far

field of the crystal and pumping with a large Gaussian beam, we can reconstruct the phase-matching function $A \text{sinc}^2(\alpha x^2 - \zeta)$ by direct imaging. The figure shows a scan of the phase-matching function with a nonlinear fit yielding $A = 93 \pm 2$ counts, $\alpha = (9.1 \pm 0.2) \times 10^{-6} \text{ mm}^2$ and $\zeta = 0.30 \pm 0.02$. Error bars are s.d. extracted from the Poissonian counting statistics and assuming as mean values the registered counts (reported as data points). **c**, Experimental correlations in the x - and y -coordinates obtained by placing the sensors in the image plane of the crystal. **d**, Example of reconstructed phase and amplitude of a biphoton state (represented in inverted HSV colours) when pumping the crystal with a superposition of LG modes: $\text{LG}_{1,3} + \text{LG}_{1,-3}$.

The coincidence count rate corresponding to a simultaneous detection of an idler photon in \mathbf{X}_1 and a signal photon in \mathbf{X}_2 is proportional to

$$\begin{aligned} \mathcal{C}(\mathbf{X}_1, \mathbf{X}_2) &:= |\langle \mathbf{X}_1, \mathbf{X}_2 | \Psi_{\text{TOT}} \rangle|^2 \\ &= |\psi_r(\mathbf{X}_1, \mathbf{X}_2) + \psi_u(\mathbf{X}_1, \mathbf{X}_2)|^2 \\ &= |\psi_r(\mathbf{X}_1, \mathbf{X}_2)|^2 + |\psi_u(\mathbf{X}_1, \mathbf{X}_2)|^2 \\ &\quad + [\psi_r^*(\mathbf{X}_1, \mathbf{X}_2)\psi_u(\mathbf{X}_1, \mathbf{X}_2) + c.c.]. \end{aligned} \quad (2)$$

The last equality displays an interference term containing the phase difference between the reference and the unknown biphoton wavefunctions.

We note that equation (2) represents an interference pattern in the four-dimensional space $(\mathbf{X}_1, \mathbf{X}_2)$. Figure 1a gives a pictorial representation of equation (2) (here considering only one coordinate per photon) for a general case in which the reference and unknown wavefunctions have a large spatial correlation spread. Although registering $\mathcal{C}(X_i, X_s)$ is enough to obtain phase information, a further visualization of the experimental interference pattern can be obtained by looking at filtered coincidence images. A coincidence image corresponds to the marginal distribution $\int \mathcal{C}(X_i, X_s) dX_a$ ($a = i$ or s) where the interference term is generically washed out. Interference in coincidence images can generally be retrieved by looking at sections of the correlation pattern, for example, extracting coincidence images from the quantity $\mathcal{C}(X_i, X_s)\delta(X_s \pm X_i)$, where the δ function represents a narrow filter applied on the four-dimensional correlation pattern (Fig. 1 shows the case $X_s = X_i$, given by the red plot). As we will demonstrate in the following section, this operation can be performed by analysing the measurements of a time-stamping camera. As shown below for the case of SPDC filtered coincidence images, besides being useful for data visualization, can allow to isolate different contributions of the biphoton state.

For the interference pattern to have a good contrast, the amplitudes of ψ_r and ψ_u have to be of a similar order. For instance, the phase of an unknown state with strong position correlations would be well resolved if the reference has the same spread of the spatial correlations, whereas the information hidden in the interference term would be more difficult to retrieve if using a reference state that is spatially uncorrelated or anticorrelated. All of these forms of correlations can be observed, in different propagation planes, within the state created in type-I SPDC by a pump beam that is well approximated by a plane wave shining a thin crystal³¹. In fact, such a state exhibits sharp correlations in the near field (that is, the image plane of the crystal) and sharp anticorrelations in the far field, while in intermediate propagation planes, one observes wider correlation patterns. Thus, one can, in principle, use this as a reference state for measuring any arbitrary two-photon state. The practical challenge would be then to find the right protocol for creating the superposition between the unknown and the reference state.

In this work we consider the case in which the unknown state is also generated in an SPDC process. In this scenario, if the pump beams used for inducing the two SPDC states are in phase, the superposition can be generated either by mixing the biphoton superposition on a beam splitter (see Supplementary Section 3) or directly inducing the two SPDC processes in the same crystal.

The simplest case of the presented scheme arises when both the reference and unknown states exhibit sharp position correlations, as is observed in the case of type-I degenerate SPDC from thin crystals. Figure 1b,c shows how the transition to a sharp correlation regime allows one to observe interference in the marginal distribution without needing post-selection on the spatial correlations. In this widely studied limit, which neglects propagation effects in the crystal volume, the two photons are created in the same transverse

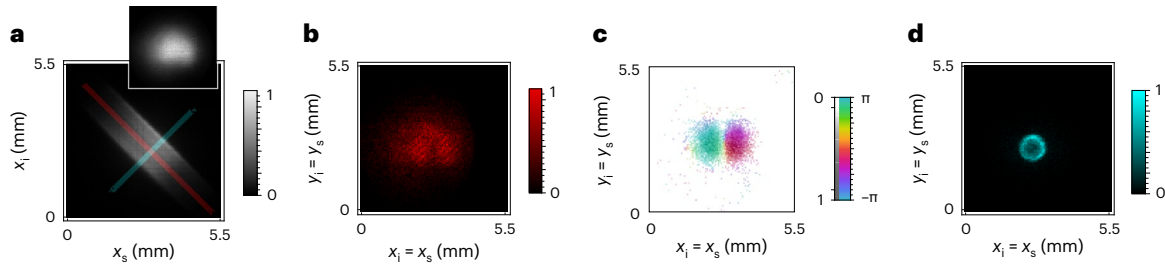


Fig. 3 | SPDC state reconstruction at an intermediate plane. a–d, When moving the camera 10 cm away from the crystal image plane, the spatial correlations are broader (as shown in **a**, for the case of x -correlations). The image obtained after post-selecting only on temporal coincidence (shown in the inset in **a**) does not exhibit any interference as in the crystal image plane. The red and cyan bands in **a** indicate the two-pixel-wide regions selected to analyse coincidence images obtained after selecting spatially correlated (**b**) and anticorrelated (**d**) photons,

respectively. The correlation image (**b**) shows again the interference between unknown and reference pump fields, allowing us to reconstruct the unknown field with off-axis holography (**c**). The anti-correlation image in **d** displays the characteristic cone shape of the phase-matching function. This function is not identical to the one obtained in Fig. 2b, but can be obtained by propagating the amplitude of the latter from the far field to the intermediate plane.

position; this means that the state can be written as (see ref. 31 and Supplementary Section 2)

$$|\Psi\rangle = \mathcal{N} \int d^2\rho \varepsilon_p(\rho) |\rho\rangle \otimes |\rho\rangle, \quad (3)$$

in the transverse coordinates of the crystal's image plane, where $\varepsilon_p(\rho)$ is the pump field on the crystal plane (the subscript p stands for pump) and \mathcal{N} is a normalization factor. The spatial correlation properties of biphoton states in this approximation are of strong interest for applications in high-dimensional quantum entanglement and quantum imaging^{32,34–36}.

If the thin-crystal approximation holds for both the reference and unknown states, equation (2) contains relevant contributions only for the case $\mathcal{C}(\mathbf{X}_1, \mathbf{X}_1)$, with $\mathbf{X}_1 = \rho$. These diagonal contributions of the coincidence count rate are given by

$$\mathcal{C}(\rho, \rho) = |\varepsilon_p(\rho) + \varepsilon_{\text{ref}}(\rho)|^2. \quad (4)$$

Here, ε_{ref} is the pump shape used to generate the reference SPDC state. Ideally, ε_{ref} can be a plane wave or, in practice, a Gaussian beam with a large waist. By controlling the reference pump beam one can map any interferometric technique that is used in classical optics for amplitude and phase reconstruction to the two-photon case. In this work, we experimentally implemented off-axis digital holography, where the reference beam is a Gaussian beam with a tilted wavefront. In off-axis digital holography, with $\varepsilon_{\text{ref}}(x, y) = A \exp(-(x^2 + y^2)/w_r^2) \exp(i2\pi(x + y)/\Lambda)$, where A is the amplitude of the reference beam, w_r the waist and $2\pi/\Lambda$ the magnitude of the average transverse wave vector components, one has

$$|\varepsilon_{\text{ref}} + \varepsilon_p|^2 = |\varepsilon_{\text{ref}}|^2 + |\varepsilon_p|^2 + 2Ae^{-\frac{r^2}{w_r^2}} \left(\varepsilon_p e^{-i2\pi\frac{(x+y)}{\Lambda}} + c.c. \right),$$

where $c.c.$ indicates the complex conjugate. From a spatial Fourier transform one can hence isolate the term proportional to ε_p and reconstruct the amplitude and phase of the unknown field. The proposed scheme can be implemented in two measurement steps: first, the correlations in the crystal image plane are measured to confirm the validity of the thin-crystal approximation, second, the coincidences corresponding to equation (4) are evaluated and the biphoton state extracted from the resulting interference pattern.

Beyond the thin-crystal approximation, one has to reconstruct also the contribution of the phase-matching function, which is in general a function of the form $\phi(\mathbf{X}_1 - \mathbf{X}_s)$. The phase-matching contribution

can be retrieved either by analysing the far field SPDC intensity distribution or, more rigorously, by post-selecting anti-diagonal correlations, that is, analysing the coincidence image $\mathcal{C}(\mathbf{X}, -\mathbf{X})$.

Experimental set-up and results

Following the theoretical description of the previous section, we experimentally implemented a platform in which, through off-axis digital holography, the biphoton state, emitted via SPDC by a type-I β -barium borate (BBO) crystal, is reconstructed. In this proof of principle experiment, we generate the unknown and reference SPDC states in the same crystal. A visual scheme of the set-up is reported in Fig. 2a (see Methods and Supplementary Section 5 for details). We built a Michelson interferometer which allowed the creation of a pump beam in the mode $\varepsilon_p + \varepsilon_{\text{ref}}$, where the reference mode is a wide Gaussian with a tilted wavefront $\varepsilon_{\text{ref}} = \exp(-r^2/w_r^2) \exp(i2\pi(x + y)/\Lambda)$, and ε_p is generated with a spatial light modulator (SLM) placed in one of the arms of the interferometer. The mean transverse momentum $2\sqrt{2}\pi/\Lambda$ is chosen to maximize the spatial resolution of the reconstructed field, and w_r is chosen to be larger than the characteristic waist parameter of ε_p , denoted as w_p . The interferometer's output is sent through the BBO crystal, and the state of the two photons is recorded using a time-stamping camera (Tpx3Cam). The camera comprises a matrix of 256×256 time-stamping pixels of $55 \mu\text{m}$ size and with ~ 1 ns time-resolution. We collected data in the crystal's image plane, which were used to reconstruct the biphoton state in the thin-crystal approximation. The emitted signal and idler photons were separated by a beam splitter and sent into different regions of the camera sensor, allowing one to check for coincidences between different pixels. In Fig. 2a we represent, for simplicity, the two sensor areas as two independent time-stamping cameras. We could verify the correctness of the thin-crystal approximation by observing the spatial correlations. This is shown by the sharp, ~ 1 -pixel-wide, spatial correlations observed in all of the cases under analysis (see Fig. 2c for an example). The data was collected in 1 min of exposure for each spatial mode under analysis. In particular, we collected both the interference pattern between the two states and a coincidence image of down-converted light induced by ε_p only. The former was used to retrieve the phase of the state under analysis, whereas the latter already gives the amplitude of the biphoton field. By exploiting this reconstruction, we were able to fully characterize the biphoton state. An example of the reconstructed phase and amplitude of the biphoton state is in Fig. 2d. Moreover, we also characterize the amplitude of the phase-matching function. To do so, we collect an image of the far field by placing an additional lens in front of the Tpx3Cam camera and entering the crystal with a wide Gaussian beam. Fitting the collected data with the function $\text{sinc}^2(\alpha x^2 - \zeta)$, α and ζ being fit parameters, we obtained $\alpha = (9.1 \pm 0.2) \times 10^{-6} \text{ mm}^2$ and

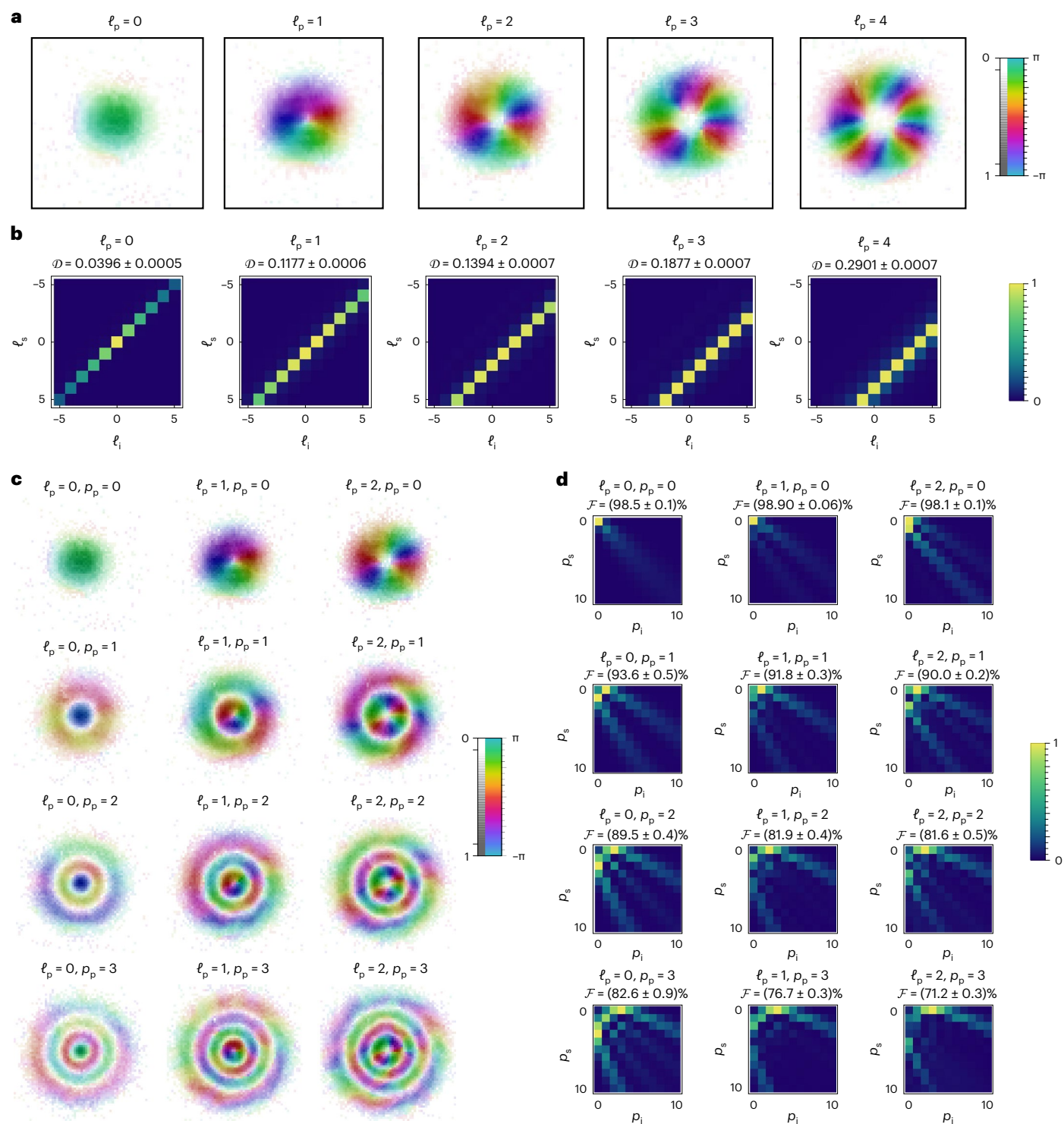


Fig. 4 | OAM and radial correlations in SPDC biphotons. Reconstructed field of the biphoton state for different OAM-carrying pump beams in $LG_{p_p=0, \ell_p}$ modes. **a**, The amplitude and phase of the state for different values of the pump OAM ℓ_p . **b**, The OAM correlations density plots of generated SPDC photons. It can be seen how increasing the pump OAM, the sum of the OAM values for the idler and signal photons shift in agreement with the conservation law of equation (6).

c, Reconstructed biphoton fields obtained by pumping the crystal with LG modes changing the ℓ and p indexes. **d**, Shows the correlations in the radial number p . In all of the plots, the OAM of signal and idler has been fixed to $\ell_i = 0, \ell_s = \ell_p$. The fidelities are obtained assuming the theoretical state calculated in the thin-crystal approximation. The error analysis is reported in Methods.

$\zeta = 0.30 \pm 0.02$. From α , we retrieve a value of the crystal length $L_{\text{exp}} = 4\omega_p \alpha / c = 0.56 \pm 0.01$ mm (where c is the speed of light in the medium), which is in very good agreement with the nominal value $L_{\text{nom}} = 0.5$ mm. The phase-matching fit is shown in Fig. 2b. This extra

measurement allows one, in principle, to evaluate corrections to the quantum state beyond the thin-crystal approximation. We took a measurement moving the camera away from the image plane of the crystal to show that our approach is not necessarily limited to sharply

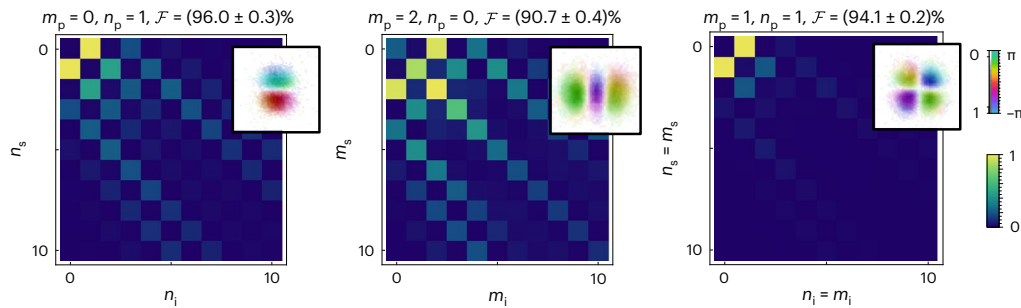


Fig. 5 | Hermite–Gauss correlations. When pumping the crystal with $\mathcal{E}_p(x, y) = \text{HG}_{m,n}(x, y)$, we observe biphoton correlations in the basis of HG modes that highlight the parity conservation of the SPDC process. Insets show the reconstructed biphoton fields from which the correlations have been

extracted. Upon each plot, the fidelity between the retrieved field and the theoretical one in the thin-crystal approximation is reported. The error analysis is discussed in Methods.

correlated photon states. In this plane, the transverse spatial correlations are broader, and the two-photon wavefunction takes the form $\phi(|\mathbf{X}_i - \mathbf{X}_s|/2)\mathcal{E}((\mathbf{X}_i + \mathbf{X}_s)/2)$ (see Supplementary Section 2 for details), where ϕ is related to the phase-matching and \mathcal{E} corresponds to the pump field propagated from the crystal to the measurement plane. As discussed in the previous section and illustrated in Fig. 1a, in this scenario, the imaging of the singles or coincidences, without any post-selection, does not show any interference (this is illustrated in inset of Fig. 3a); however, when we look at the coincidence image after selecting diagonal spatial correlations, we obtain the marginal $\int d^2\mathbf{X}_s \mathcal{C}(\mathbf{X}_i, \mathbf{X}_s)\delta(\mathbf{X}_s - \mathbf{X}_i) = |\mathcal{E}(\mathbf{X}_i)|^2|\phi(0)|^2$. In our case, $\mathcal{E} = \mathcal{E}_p + \mathcal{E}_{\text{ref}}$ and we therefore see the interference between reference and unknown pump beam (see Fig. 3b). From this pattern, one can reconstruct the pump field contribution to the SPDC state, as shown in Fig. 3c. This reconstruction yields only the part of the biphoton state associated with the pump field; however, the phase-matching can also be reconstructed from the same measurement by extracting $\int \mathcal{C}(\mathbf{X}_i, \mathbf{X}_s)\delta(\mathbf{X}_i + \mathbf{X}_s)d\mathbf{X}_s = |\mathcal{E}(0)|^2|\phi(\mathbf{X}_i)|^2$ (see Fig. 3b). We note that in our set-up, the phase-matching functions of reference and unknown state are identical, so we only have access to the absolute value of this contribution. It must be noted, however, that a set-up in which the two SPDC states are created from two independent sources would also allow access to eventual phase structures in the phase-matching term (see Supplementary Section 3). Alternatively, one can extract the phase-matching contribution at different planes and infer its phase using the Gerchberg–Saxton algorithm³⁷. We will investigate this non-interferometric approach in a future work. Once the biphoton state is given, one can extract any desired information about this state, for example, correlations in different degrees of freedom, entanglement and the decomposition in arbitrary sets of spatial modes.

Reconstruction of spatial mode correlations

One of the degrees of freedom of light that has been extensively studied for high-dimensional quantum applications, is the OAM. Modes in OAM eigenstates are represented by wavefunctions possessing a phase term of the form $\exp(i\ell\phi)$ in position representation. Here, ϕ is the azimuthal angle in cylindrical coordinates, and $\ell \in \mathbb{Z}$ is the OAM value (along the propagation direction) in units of \hbar carried by a photon in such a state. Given a set of OAM-carrying modes $\langle r, \phi|p, \ell \rangle := f_p(r)\exp(i\ell\phi)$, where $f_p(r)$ denotes an orthonormal set of radial functions, the probability of detecting the idler photon with OAM ℓ_i and the signal with OAM ℓ_s is (for fixed p_i and p_s)

$$P_{\ell_i, \ell_s}^{p_i, p_s} = \left| \iint \mathcal{E}_p(r, \phi) f_{p_i}^*(r) f_{p_s}^*(r) e^{-i(\ell_i + \ell_s)\phi} r dr d\phi \right|^2 \quad (5)$$

In particular, when the pump beam carries an OAM equal to ℓ_p one has the OAM conservation law:

$$\ell_p = \ell_i + \ell_s, \quad (6)$$

which can be immediately deduced from equation (5)³¹ and was first demonstrated in ref. 32. We investigated this relationship for several OAM values by entering the crystal with LG modes³⁸. These are a set of modes defined as:

$$\text{LG}_{p,\ell}(r, \phi) := \langle r, \phi|p, \ell \rangle \propto (r/w)^{|\ell|} L_p^{|\ell|} (2r^2/w^2) \exp(-(r/w)^2) \exp(i\ell\phi),$$

where $L_p^{|\ell|}(x)$ are associated Laguerre polynomials. LG modes are cylindrically symmetric modes carrying OAM and with minimal divergence in free space³⁹. We analysed the case in which we entered the crystal with states having azimuthal index $\ell \in \{0, 1, 2, 3, 4\}$, the results are reported in Fig. 4. We show the OAM detection probabilities without specifying the radial function, calculated as $P_{\ell_i, \ell_s}^{p_i, p_s} = \sum_{p_i, \ell_i} \sum_{p_s, \ell_s} P_{\ell_i, \ell_s}^{p_i, p_s}$, where we restricted the sums over the radial indexes for $p_{i,s} = 0, \dots, 10$. It is evident how increasing the OAM carried by the pump causes the OAM correlations to shift in agreement with equation (6) (as also observed in, for example, ref. 32). It has been observed that the SPDC state in the OAM basis violates high-dimensional Bell inequalities^{33,40}. In Fig. 4b, we also report the trace distances between the theoretically calculated ($P_{\ell_i, \ell_s}^{\text{th}}$) and reconstructed (P_{ℓ_i, ℓ_s}) probability distributions, defined as $\mathcal{D} = \sum_{\ell_i, \ell_s} |P_{\ell_i, \ell_s} - P_{\ell_i, \ell_s}^{\text{th}}|/2$. The values of \mathcal{D} increase with a higher ℓ_p , mainly due to imperfections in the pump preparations (hence the pump beam is better described as a superposition of OAM states). The distributions $P_{\ell_i, \ell_s}^{\text{th}}$ are shown in Supplementary Fig. 4.

The radial index $p \in \mathbb{N}$ of LG modes corresponds to the number of radial zeros and can be treated as a quantum number^{41,42}. In Fig. 4c, experimental results of biphoton states for pump beams, prepared as LG modes, are shown. The coefficients of the SPDC state decomposition in LG modes $|\Psi\rangle = \sum_{p_i, \ell_i} \sum_{p_s, \ell_s} C_{p_i, \ell_i}^{p_s, \ell_s} |p_i, \ell_i\rangle \otimes |p_s, \ell_s\rangle$ were extracted from the reconstructed states. Figure 4d shows experimental correlations in radial indexes (with OAM indexes of idler and signal fixed as $\ell_i = 0, \ell_s = \ell_p$). When choosing the waist parameter of the decomposition to be equal to the pump waist, the correlations are maximized for $p_{i,s} = p_p, p_{s,i} = 0$. This can be understood from the similarity between the integral expression of $C_{p_i, \ell_i}^{p_s, \ell_s}$ and the orthogonality relationship of LG modes. The fidelity $\mathcal{F} = |\sum_{p_i} C_{p_i, 0}^{p_s, \ell_p} C_{p_i, 0}^{\text{th}, p_s, \ell_p}|^2$ was evaluated within the considered subspaces (where indices $p_{i,s}$ are bounded from 0 to 10 and $\ell_i = 0, \ell_s = \ell_p$), where $C_{p_i, 0}^{p_s, \ell_p}$ represents the measured coefficients and $C_{p_i, 0}^{\text{th}, p_s, \ell_p}$ represents those expected from the thin-crystal

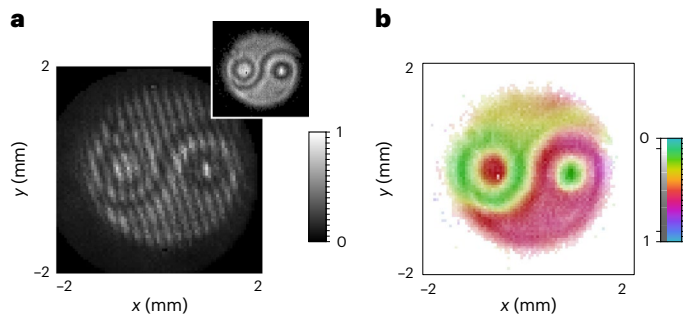


Fig. 6 | Image reconstruction. **a**, Coincidence image of interference between a reference SPDC state and a state obtained by a pump beam with the shape of a Ying and Yang symbol (shown in the inset). The inset scale is the same as in the main plot. **b**, Reconstructed amplitude and phase structure of the image imprinted on the unknown pump.

approximation—both of the coefficients are obtained after normalizing the state in the reduced subspace.

In this approximation, the parity of the spatial modes is also conserved³⁵. This effect can be highlighted by considering pump beams in HG modes³⁸ which, on the crystal plane, read

$$\begin{aligned} \text{HG}_{m_p, n_p}(x, y) &:= \langle x, y | m_p, n_p \rangle \\ &\propto \exp\left(-\frac{x^2 + y^2}{w_p^2}\right) h_{m_p}(x/w_p) h_{n_p}(y/w_p), \end{aligned}$$

where $h_m(x)$ represents Hermite polynomials of order m . HG modes form a complete, orthonormal set with even or odd functions along the x - or y -directions; the SPDC state can therefore be decomposed as $|\Psi\rangle = \sum_{m_i, n_i} K_{m_i, n_i}^{m_s, n_s} |m_i, n_i\rangle \otimes |m_s, n_s\rangle$. This basis has been extensively studied^{35,36,43} and recently considered for biphoton super-resolution measurements⁴⁴. When studying the SPDC correlations on the basis of HG modes (chosen with the same waist parameter $w = w_p$ of the pump), one has the conservation laws: $n_p = \text{mod}(n_i + n_s, 2)$ and $m_p = \text{mod}(m_i + m_s, 2)$, as can be directly inferred from the parity of the integrands appearing in the expression of $K_{m_i, n_i}^{m_s, n_s}$ (see Methods and ref. 35 for a detailed proof). Figure 5 shows calculated HG mode correlations for different states (with reconstructed biphoton amplitude and phase shown in the insets). The results show an excellent agreement with theory; in particular, the parity conservation is evident from the chessboard-like correlation patterns.

Finally, Fig. 6 demonstrates an example of the potential applications of biphoton digital holography. The unknown pump beam can carry information about an image or be scattered by a three-dimensional object. The information about the scatterer is transferred to the SPDC state and can be retrieved through our technique (Fig. 6b). We show this in the case of off-axis holography, which can present limitations for complex structures due to the limited camera resolution. These limitations are not related to our proposal and can be improved by employing other approaches, for example, on-axis phase-shifting digital holography⁹.

Conclusion

In this work we introduced a novel approach for reconstructing the spatial structure of correlated two photons states. Our proposal exploits the coherent superposition of two SPDC states and the possibility of imaging the amplitude of this superposition with a time-stamping camera. The experimental results showed how, from a single measurement, it is possible to retrieve, in post-processing, a large amount of information about a two-photon spatial state, including correlations in different degrees of freedom, entanglement and spatial mode decomposition in arbitrary bases. We focused on the simple case of SPDC

generated from thin crystals and, for different pump fields, analysed OAM and parity conservation, high-dimensional entangled states and radial mode correlations. The results show the superiority of this technique, compared with projective techniques (for example, the ones in refs. 34,42,45), in the context of benchmarking highly correlated quantum states. We observe that, if a projective measurement was performed on a 11×11 subspace, in line with the ones considered in this work for radial modes, several days would be required to accumulate the necessary statistics on 121^2 projections due to the low count rates associated with the lossy techniques used for mode projection. In comparison, our approach allows us to obtain the necessary data in a few minutes, independently from the dimensionality of the subspace to be analysed (the latter is only limited by the camera resolution). We also note that, with the time-stamping camera, when spatial correlations are present, a further background subtraction is possible thus improving the signal-to-noise ratio of this kind of measurement. We thus achieved a three-order-of-magnitude enhancement on the reconstruction time with high fidelities for the biphoton states, obtaining an average fidelity equal to 87%. The lowest fidelity values are due to imperfect pump preparations or an undesired spatially varying phase in the reference beam and not to intrinsic limitations of the technique. Although most of our results are based on a specific kind of two-photon state, we also showed how it is possible to generalize to states where the correlations are not sharp. A key ingredient is to generate reference states with spatial correlations that overlap well with the correlations in the unknown state. Future investigations will be devoted to the generalization of this approach to arbitrary two and multiphoton states, realizing experiments where the reference and unknown states are generated from distant sources. Moreover, we point out that the same technique presented here can be applied to measure biphoton states in the time-frequency degrees of freedom, where several interferometric approaches have been demonstrated^{46–48}. Besides the quantum state reconstruction, future investigations will be devoted to the generalization of our protocol to imaging experiments.

Online content

Any methods, additional references, Nature Portfolio reporting summaries, source data, extended data, supplementary information, acknowledgements, peer review information; details of author contributions and competing interests; and statements of data and code availability are available at <https://doi.org/10.1038/s41566-023-01272-3>.

References

1. Flamini, F., Spagnolo, N. & Sciarrino, F. Photonic quantum information processing: a review. *Rep. Prog. Phys.* **82**, 016001 (2018).
2. Nielsen, M. A. & Chuang, I. *Quantum Computation and Quantum Information* (Cambridge Univ. Press, 2002).
3. Huszár, F. & Houlby, N. M. T. Adaptive bayesian quantum tomography. *Phys. Rev. A* **85**, 052120 (2012).
4. Mahler, D. H. et al. Adaptive quantum state tomography improves accuracy quadratically. *Phys. Rev. Lett.* **111**, 183601 (2013).
5. Rambach, M. et al. Robust and efficient high-dimensional quantum state tomography. *Phys. Rev. Lett.* **126**, 100402 (2021).
6. Gross, D., Liu, Y.-K., Flammia, S. T., Becker, S. & Eisert, J. Quantum state tomography via compressed sensing. *Phys. Rev. Lett.* **105**, 150401 (2010).
7. Bouchard, F. et al. Compressed sensing of twisted photons. *Opt. Express* **27**, 17426–17434 (2019).
8. Bent, N. et al. Experimental realization of quantum tomography of photonic qudits via symmetric informationally complete positive operator-valued measures. *Phys. Rev. X* **5**, 041006 (2015).
9. Yamaguchi, I. in *Digital Holography and Three-Dimensional Display* (ed. Poon, T.-C.) 145–171 (Springer, 2006).

10. Verrier, N. & Atlan, M. Off-axis digital hologram reconstruction: some practical considerations. *Appl. Optics* **50**, H136–H146 (2011).
11. D’Errico, A., D’Amelio, R., Piccirillo, B., Cardano, F. & Marrucci, L. Measuring the complex orbital angular momentum spectrum and spatial mode decomposition of structured light beams. *Optica* **4**, 1350–1357 (2017).
12. Brida, G., Genovese, M. & Ruo Berchera, I. Experimental realization of sub-shot-noise quantum imaging. *Nat. Photon.* **4**, 227–230 (2010).
13. Bolduc, E., Faccio, D. & Leach, J. Acquisition of multiple photon pairs with an EMCCD camera. *J. Opt.* **19**, 054006 (2017).
14. Unternährer, M., Bessire, B., Gasparini, L., Perenzoni, M. & Stefanov, A. Super-resolution quantum imaging at the heisenberg limit. *Optica* **5**, 1150–1154 (2018).
15. Zarghami, M. et al. A 32×32-pixel CMOS imager for quantum optics with per-SPAD TDC, 19.48 fill-factor in a 44.64- μm pitch reaching 1-MHz observation rate. *IEEE J. Solid State Circuits* **55**, 2819–2830 (2020).
16. Eckmann, B. et al. Characterization of space-momentum entangled photons with a time resolving CMOS SPAD array. *Opt. Express* **28**, 31553–31571 (2020).
17. Fisher-Levine, M. & Nomerotski, A. TimepixCam: a fast optical imager with time-stamping. *J. Instrum.* **11**, C03016 (2016).
18. Nomerotski, A. et al. Intensified Tpx3Cam, a fast data-driven optical camera with nanosecond timing resolution for single photon detection in quantum applications. *J. Instrum.* **18**, C01023 (2023).
19. Moreau, P.-A., Toninelli, E., Gregory, T. & Padgett, M. J. Imaging with quantum states of light. *Nat. Rev. Phys.* **1**, 367–380 (2019).
20. Toninelli, E. et al. Resolution-enhanced quantum imaging by centroid estimation of biphotons. *Optica* **6**, 347–353 (2019).
21. Defienne, H. et al. Pixel super-resolution with spatially entangled photons. *Nat. Commun.* **13**, 3566 (2022).
22. Boucher, P., Defienne, H. & Gigan, S. Engineering spatial correlations of entangled photon pairs by pump beam shaping. *Opt. Lett.* **46**, 4200–4203 (2021).
23. Devaux, F., Mosset, A., Moreau, P.-A. & Lantz, E. Imaging spatiotemporal Hong–Ou–Mandel interference of biphoton states of extremely high Schmidt number. *Phys. Rev. X* **10**, 031031 (2020).
24. Zhang, Y., England, D., Nomerotski, A. & Sussman, B. High speed imaging of spectral-temporal correlations in Hong–Ou–Mandel interference. *Opt. Express* **29**, 28217–28227 (2021).
25. Gao, X., Zhang, Y., D’Errico, A., Heshami, K. & Karimi, E. High-speed imaging of spatiotemporal correlations in Hong–Ou–Mandel interference. *Opt. Express* **30**, 19456–19464 (2022).
26. Moreau, P.-A. et al. Imaging Bell-type nonlocal behavior. *Sci. Adv.* **5**, eaaw2563 (2019).
27. Defienne, H., Ndagano, B., Lyons, A. & Faccio, D. Polarization entanglement-enabled quantum holography. *Nat. Phys.* **17**, 591–597 (2021).
28. Töpfer, S. et al. Quantum holography with undetected light. *Sci. Adv.* **8**, eabl4301 (2022).
29. Thekkadath, G. S. et al. Intensity interferometry for holography with quantum and classical light. *Sci. Adv.* **9**, adh1439 (2023).
30. Parniak, M. et al. Wavevector multiplexed atomic quantum memory via spatially-resolved single-photon detection. *Nat. Commun.* **8**, 2140 (2017).
31. Walborn, S. P., Monken, C. H., Pádua, S. & Ribeiro, P. H. Souto Spatial correlations in parametric down-conversion. *Phys. Rep.* **495**, 87–139 (2010).
32. Mair, A., Vaziri, A., Weihs, G. & Zeilinger, A. Entanglement of the orbital angular momentum states of photons. *Nature* **412**, 313 (2001).
33. Agnew, M., Leach, J., McLaren, M., Roux, F. S. & Boyd, R. W. Tomography of the quantum state of photons entangled in high dimensions. *Phys. Rev. A* **84**, 062101 (2011).
34. D’Errico, A., Hufnagel, F., Miatto, F., Rezaee, M. & Karimi, E. Full-mode characterization of correlated photon pairs generated in spontaneous downconversion. *Opt. Lett.* **46**, 2388–2391 (2021).
35. Walborn, S. P., Pádua, S. & Monken, C. H. Conservation and entanglement of Hermite–Gaussian modes in parametric down-conversion. *Phys. Rev. A* **71**, 053812 (2005).
36. Miatto, F. M., di Lorenzo Pires, H., Barnett, S. M. & van Exter, M. P. Spatial Schmidt modes generated in parametric down-conversion. *Eur. Phys. J. D* **66**, 263 (2012).
37. Gerhberg, R. W. & Saxton, W. O. A practical algorithm for the determination of phase from image and diffraction plane picture. *Optik* **35**, 237–246 (1972).
38. Siegman, A. E. *Lasers* (Univ. Science Books, 1986).
39. Vallone, G. et al. General theorem on the divergence of vortex beams. *Phys. Rev. A* **94**, 023802 (2016).
40. Dada, A. C., Leach, J., Buller, G. S., Padgett, M. J. & Andersson, E. Experimental high-dimensional two-photon entanglement and violations of generalized Bell inequalities. *Nature Physics* **7**, 677–680 (2011).
41. Karimi, E. et al. Radial quantum number of Laguerre–Gauss modes. *Phys. Rev. A* **89**, 063813 (2014).
42. Zhang, D., Qiu, X., Zhang, W. & Chen, L. Violation of a Bell inequality in two-dimensional state spaces for radial quantum number. *Phys. Rev. A* **98**, 042134 (2018).
43. Zhang, Y. et al. Hong–Ou–Mandel interference of entangled hermite-gauss modes. *Phys. Rev. A* **94**, 033855 (2016).
44. Grenapin, F. et al. Super-resolution enhancement in bi-photon spatial mode demultiplexin. Preprint at <https://arxiv.org/abs/2212.10468> (2022).
45. Valencia, N. H., Srivastav, V., Leedumrongwatthanakun, S., McCutcheon, W. & Malik, M. Entangled ripples and twists of light: radial and azimuthal Laguerre–Gaussian mode entanglement. *J. Optics* **23**, 104001 (2021).
46. Jin, R.-B. & Shimizu, R. Extended Wiener–Khinchin theorem for quantum spectral analysis. *Optica* **5**, 93–98 (2018).
47. Borghi, M. Phase-resolved joint spectra tomography of a ring resonator photon pair source using a silicon photonic chip. *Opt. Express* **28**, 7442–7462 (2020).
48. Faruque, I. I. et al. Quantum-referenced spontaneous emission tomography. Preprint at <https://arxiv.org/abs/2212.12521> (2022).

Publisher’s note Springer Nature remains neutral with regard to jurisdictional claims in published maps and institutional affiliations.

Open Access This article is licensed under a Creative Commons Attribution 4.0 International License, which permits use, sharing, adaptation, distribution and reproduction in any medium or format, as long as you give appropriate credit to the original author(s) and the source, provide a link to the Creative Commons license, and indicate if changes were made. The images or other third party material in this article are included in the article’s Creative Commons license, unless indicated otherwise in a credit line to the material. If material is not included in the article’s Creative Commons license and your intended use is not permitted by statutory regulation or exceeds the permitted use, you will need to obtain permission directly from the copyright holder. To view a copy of this license, visit <http://creativecommons.org/licenses/by/4.0/>.

© The Author(s) 2023, corrected publication 2023

Methods

Detailed experimental set-up

A Gaussian beam with a wavelength of 405 nm is produced through the second harmonic generation of a 810 nm pulsed Ti:Sa laser (Chameleon Vision II), the latter has a pulse duration of 150 fs and a repetition rate of 80 MHz. The beam is magnified to ~1 cm beam waist and sent in the input of a Michelson interferometer. A reflective liquid crystal SLM is placed in one arm of the interferometer. At the interferometer output, all of the diffraction orders of the SLM, except for the first, are filtered out by a slit placed in the SLM's Fourier plane. The slit allows keeping the reference beam (corresponding to the beam going through the interferometer arm without the SLM) with a different transverse wavevector, thus allowing to perform off-axis digital holography while maintaining good interference stability. The phase masks applied on the SLM allows the generation of arbitrary optical fields by means of the technique introduced in ref. 49. After filtering, both beams (each with the power of the order of 100 mW) are collimated and sent on the 0.5-mm-thick type-I BBO crystal for SPDC generation. The vertically polarized down-converted light is collimated by a lens of focal length $f = 25$ cm, and split into two copies, that is signal and idler photons are sent to two separate paths (with 50% probability), by a sequence consisting of a half-wave plate rotated by 22.5° and a polarizing beam splitter (effectively working as an ordinary beam splitter). The two copies are sent on parallel paths (by sending them on another polarizing beam splitter and changing the polarizations in such a way as to maximize the intensity on one output port). The two beams have a lateral shift, that avoids them from being overlapped, and are focused, by means of a $f = 50$ cm lens in the thin-crystal approximation configuration and by a $f = 75$ cm lens for the reconstruction of the state in an intermediate plane, on the TPX3CAM sensor. In front of the sensor, a 3 nm bandpass filter is applied to ensure the frequency degeneracy of the analysed photons. The bandpass filter also ensures a sufficient contrast of the interference fringes. In the far field configuration, used to reconstruct the phase-matching function, an additional $f = 20$ cm lens is placed in front of the camera in a confocal configuration.

Data acquisition and analysis

The data was acquired by collecting SPDC light on the Tpx3Cam for 1 min for each dataset. We collected data for scenarios in which both the reference and pump beams were sent via the BBO crystal, and cases in which only the pump beam was sent via the crystal, after blocking the reference arm. The acquired data files report the time stamp at which the counts were detected (see refs. 17,24,25,50 for more information). In our case, as we shine two copies of the SPDC light on different regions on the camera, we can have counts from these regions detected in the same time window. We considered as coincidences the counts from the two regions with a time-stamp difference of 5 ns. We analysed the spatial correlations from this set of counts, confirming the validity of the thin-crystal approximation. A weak constant background in the correlation plot is always present (due to dark counts and background light) and can be reduced by removing the counts outside the correlation region. Coincidence images were obtained by plotting the positions of the counts selected as coincidences.

The resulting coincidence images were analysed using standard off-axis digital holography⁹, as described in the main text. The decomposition of the reconstructed states in terms of OAM, HG and LG modes has been conducted by direct calculations of the expansion coefficients in the respective bases. The errors on the fidelities have been obtained by repeating the analysis for different state reconstructions, where the original coincidence images were modified pixel by pixel by random amounts within the uncertainty, given by the square root of the coincidences assuming Poissonian statistics. In the main text, we report the average fidelity and the standard deviation over twenty different realizations.

Parity conservation

The coefficients $K_{m_i, n_i}^{m_s, n_s}$ in the HG expansion of the SPDC state are given by the integral

$$K_{m_i, n_i}^{m_s, n_s} := \langle (m_i, n_i | \otimes (m_s, n_s) | \Psi \rangle = \mathcal{N} \iint \mathcal{E}(x, y) e^{-2\left(\frac{x}{w_p}\right)^2} h_{m_i}\left(\frac{x}{w_p}\right) h_{m_s}\left(\frac{x}{w_p}\right) \times e^{-2\left(\frac{y}{w_p}\right)^2} h_{n_i}\left(\frac{y}{w_p}\right) h_{n_s}\left(\frac{y}{w_p}\right) dx dy.$$

We consider the case in which $\mathcal{E}(x, y) = F_x(x)F_y(y)$ where F_x and F_y are even or odd functions of x and y , respectively (which is the case if the pump is in a HG mode). We have $C_{m_i, n_i}^{m_s, n_s} = I_{F_x} \times I_{F_y}$, where

$$I_{F_\xi} := \sqrt{\mathcal{N}} \int_{-\infty}^{\infty} e^{-2\left(\frac{\xi}{w_p}\right)^2} F_\xi(\xi) h_{l_i}\left(\frac{\xi}{w_p}\right) h_{l_s}\left(\frac{\xi}{w_p}\right) d\xi$$

with $l = m, n$ for $\xi = x, y$, respectively. The product $h_{l_i}\left(\frac{\xi}{w_p}\right) h_{l_s}\left(\frac{\xi}{w_p}\right)$ is even/odd if $l_i + l_s$ is even/odd. Thus, the integral is zero if the parity of F_ξ is different than the parity of $l_i + l_s$, hence the conservation law mentioned in the main text.

Data availability

The data that support the findings of this study are available from the corresponding author upon reasonable request.

Code availability

The code used for the data analysis is available from the corresponding author upon reasonable request.

References

- Bolduc, E., Bent, N., Santamato, E., Karimi, E. & Boyd, R. W. Exact solution to simultaneous intensity and phase encryption with a single phase-only hologram. *Opt. Lett.* **38**, 3546–3549 (2013).
- Zhang, Y., Orth, A., England, D. & Sussman, B. Ray tracing with quantum correlated photons to image a three-dimensional scene. *Phys. Rev. A* **105**, L011701 (2022).

Acknowledgements

We would like to acknowledge Y. Zhang for providing the LabView code to analyse the data extracted from the time-stamping camera. This work was supported by Canada Research Chairs (CRC), Canada First Research Excellence Fund (CFREF) Program, NRC-uOttawa Joint Centre for Extreme Quantum Photonics (JCEP) via the High Throughput and Secure Networks Challenge Program at the National Research Council of Canada. D.Z. and F.S. acknowledge support from the ERC Advanced Grant QU-BOSS (grant agreement no. 884676) and “bando per il finanziamento di progetti di ricerca congiunti ed individuali per la mobilità all'estero di studenti di dottorato” issued by Sapienza.

Author contributions

A.D. conceived the idea. D.Z., N.D. and A.D. devised the experimental set-up. D.Z., N.D. and A.D. performed the experiment. D.Z. analysed the data. N.D. analysed the spatial mode correlations. E.K. and F.S. supervised the project. D.Z., N.D. and A.D. prepared the first version of the paper. All authors contributed to the writing of the paper.

Competing interests

The authors declare no competing interests.

Additional information

Supplementary information The online version contains supplementary material available at <https://doi.org/10.1038/s41566-023-01272-3>.

Correspondence and requests for materials should be addressed to Alessio D'Errico.

Peer review information *Nature Photonics* thanks Will McCutcheon and the other, anonymous, reviewer(s) for their contribution to the peer review of this work.

Reprints and permissions information is available at www.nature.com/reprints.